EARTHQUAKE ENGINEERING AND STRUCTURAL DYNAMICS
Earthquake Engng Struct. Dyn. 2001; **30**:213–235

Feedback–feedforward control of offshore platforms under random waves

J. Suhardjo[1] and A. Kareem[2,*]

[1] *Office of Information Technologies, University of Notre Dame, Notre Dame, IN, U.S.A.*
[2] *Department of Civil Engineering and Geological Sciences, University of Notre Dame, Notre Dame, IN, U.S.A.*

SUMMARY

This study investigates the control of jacket-type offshore platforms. The deck displacement of jacket-type offshore platforms can be controlled using both passive and active control mechanisms. Among the passive control mechanisms, a tuned mass damper concept is studied in this paper. Active control mechanisms considered here include the active mass damper, the active tendon mechanism and the propeller thruster. An optimal frequency domain approach to active control of wave-excited platforms is used in which the H_2 norm of the transfer function from the external disturbance to the regulated output is minimized. In this study, the hydrodynamic drag force is evaluated using the JONSWAP wave spectrum. Unlike conventional linearization approaches, the influence of non-linearity in the drag force is retained in this scheme by expressing the non-linear force components in terms of higher-order convolutions of the water-particle velocities. To demonstrate the effectiveness of this scheme, the platform performance with and without control devices under different sea states is evaluated. It is demonstrated that the control devices are useful in reducing the displacement response of jacket-type offshore platforms, especially when the wave forces are concentrated at frequencies close to the natural frequencies of the platform. This becomes especially significant in deep waters because the natural frequencies of jacket-type platforms fall closer to the dominant wave frequencies in deep waters. Adding control devices to deep water platforms will ensure a reduction both in the global response of the platform and in localized effects, such as the fatigue of welded joints. Copyright © 2001 John Wiley & Sons, Ltd.

KEY WORDS: feedback–forward control; offshore platforms; random waves

INTRODUCTION

As the amount of oil near the shores decreases, the need to tap oil resources located in deep waters or hostile environments increases. Therefore, improvements in the design and

* Correspondence to: A. Kareem, Department of Civil Engineering and Geological Sciences, University of Notre Dame, 156 Fitzpatrick Hall, Notre Dame, Indiana 46556-5602, U.S.A.

Contract/grant sponsor: National Science Foundation Grants; Contract/grant no: BCS 90-96274, CMS 95-03779.
Contract/grant sponsor: Office of Naval Research Grant & Several Oil Companies; Contract/grant no: N 00014-93-1-0761.

Received 28 September 1999
Revised 25 May 2000
Accepted 5 June 2000

construction practices of offshore drilling and production platforms are necessary [1]. It is essential that these platforms be able to withstand the action of wind, waves and earthquakes under both operating and extreme conditions.

In deep water, the natural frequencies of conventional gravity type platforms are within the range of everyday wave heights. This results in excessive fatigue-related damage to the platform. In the case of extreme waves in deep water offshore platforms can experience large motions. Excessive motions of the platforms can threaten their safety and operation [2]. To prevent fatigue damage and protect the operations and crew of the platform, a number of design modifications have been introduced to limit such impacts. These modifications include utilizing compliant platforms (e.g. guyed towers and tension leg platforms). Other possibilities involving implementation of control devices exist to reduce both fatigue effects and survival during extreme events. Despite the rich tradition of active control systems in the dynamic positioning of drilling ships, control devices have not been actively pursued by the offshore industry. This may be attributed to deck space being at a premium, needs for temperature control of energy-dissipating fluids and power and maintenance requirements of an active system. In civil engineering literature, few studies have been conducted using active control devices in offshore structures [2–9]. However, with recent success and burgeoning growth in the application of active systems in land-based structures such as tall buildings, TV towers and other structures, interest in these devices for possible application to offshore structures is receiving more attention [10–13].

There are two types of devices that can be used to control structural response, i.e. passive and active. Passive control devices utilize the dynamics of the structure itself to dissipate energy. One passive control device that can be used to control the structural response of offshore platforms is the tuned mass damper (TMD). The TMD is commonly used for the control of tall buildings under wind excitation [11, 12, 14]. The secondary mass of inertial type damping devices such as a TMD can be replaced by a water tank in which the sloshing of liquid mimics the actions of a TMD consisting of a mass damper and spring system. However, the ability of a passive device to control the response of a structure is limited, and the device can generally be tuned to only one of the structure's natural frequencies.

The limitations that are inherent in passive devices can be overcome by using an active control device. Active control devices utilize an external power source to generate forces which control the structure. These generated forces are called control forces. Active control mechanisms that can be used in offshore structures include the active mass damper (AMD), the active tendon system and the propeller thruster. One type of active control device that has received some recent attention for offshore platforms is the thruster-assisted mooring system [8, 9]. Mooring systems help to maintain the general position of the platform. However, even with a mooring system, a platform may be susceptible to slow drift oscillations caused by currents and wind. To counteract such motion, thrusters can be added to the mooring system. Therefore, attention has been given to designing a thruster-assisted mooring system which can limit the motions caused by currents and wind. Another active control device that has been studied is active pneumatic control [2]. This device limits the deflections of a platform by individually controlling the air pressure inside air tanks located at the bottom of the platform.

In this paper, a jacket-type platform under random seas is used to demonstrate the effectiveness of various control devices. The analysis in this study is based on a frequency domain approach that minimizes the H_2 norm of the transfer function from the external disturbance to the regulated output [6, 15–17]. The displacement of the platform deck is controlled using

both passive and active control mechanisms. The approach presented in this paper includes a feedforward–feedback linkage which enhances performance of the controller.

THEORETICAL BACKGROUND

A state-space representation of wave load effects is presented in this section. This is followed by brief theoretical background concerning frequency-domain-based H_2 control, and its solution procedure. An example is then presented to illustrate the procedure and to evaluate the performance of different systems.

STATE–SPACE MODELLING OF WAVE LOAD EFFECTS — FEEDFORWARD LINK

In control theory, the equations of motion of a system are frequently represented using a state-space description. This general representation is readily applicable in numerical algorithms for analysis and synthesis. In structural control, the state vector is typically a $2n$-dimensional vector of displacements and velocities for an n-degree-of-freedom structure. Similarly, the external loading needs to be expressed in the state-space framework, which is then combined with the structural model for the control system design and analysis.

In many cases, the spectral properties of the environmental loadings on a structure are known and can be modelled. By including such models in the control design, better control of the structure can be obtained using little additional effort. The feedforward links can be formulated using two types of input. First, the feedforward link can be based on established spectral characteristics of an excitation such as earthquakes, winds or waves [16, 18, 19]. Second, the feedforward loops can be configured based on actual real-time measurements by fitting models such as the auto-regressive (AR) model to data [20, 21]. A feedback–feedforward control scheme includes a stochastic model of the external disturbance in the control design (e.g. References [16, 19]). In these studies, the external disturbance was an earthquake ground acceleration and wind velocity fluctuations, respectively. The equations of motion of the structural system were augmented with appropriate earthquake and wind excitation models obtained by filtering a Gaussian white noise process. The augmented equations of motion were then used to determine a control which utilized both feedback and feedforward compensation. The feedback loop incorporated measurements of the response of the structure into the control law. The information from both the structure and the excitation was utilized in the feedforward control law with an observer designed to estimate the states of the external excitation model based upon the base acceleration or mean wind speed information. Yamada and Kobori [20] and Mei *et al.* [21] utilized real-time measurements of earthquakes and fitted these in terms of AR models. These models were augmented with structural models for real-time control force calculation. The latter approach offers a more robust feedforward input as it is not based on a pre-defined spectral description. Rather, it adjusts to reflect the nature of actual measured input. In the following discussion, a state-space representation for wave load effects is presented.

Power spectral density functions of wave forces

The wave-induced loads on structures are given by the Morison equation [22]. This equation has an inertial force term and a drag term. The latter contains a non-linear term involving the

water-particle velocity. Historically, analyses of non-linear systems in the frequency domain have been based on the statistical linearization approach (e.g. References [23, 24]). However, the commonly used method of equivalent linearization fails to capture the higher-order statistics of the response, i.e. its non-Gaussian characteristics. In addition, response energy in frequency ranges outside that of the input spectrum is not observed using this technique.

In this study, an enhanced linearization approach is utilized which permits the loading spectral description to reveal spectral peaks outside the range of input frequencies that are undetectable using conventional linearization techniques. The enhanced approach involves casting spectral descriptions of the drag force by a series of convolutions involving water-particle velocity spectra [25–27].

Investigations of the dynamics of jacket-type platforms indicate that the quadratic dependence of the drag force on the water-particle velocity leads to significant excitation near one of the platform resonant frequencies, and thus results in an appreciable increase in the platform response — a phenomenon that is captured in this study.

Following the enhanced linearization scheme discussed above, the hydrodynamic wave loads acting on a typical offshore platform can be expressed as

$$F_{\text{wave}}(t) = F_{\text{inertia}}(t) + F_{\text{linear}_{\text{drag}}}(t) + F_{\text{current}}(t) + F_{\text{non-linear}_{\text{drag}}}(t) \tag{1}$$

where F_{inertia} is the inertia force, $F_{\text{linear}_{\text{drag}}}$ is the linear part of the wave drag force, F_{current} is the force created by the current and $F_{\text{non-linear}_{\text{drag}}}$ is the non-linear part of the wave drag force. Each component of the force is expressed in terms of the wave height fluctuation. Accordingly, their corresponding spectral density functions can be related.

One of the most commonly used spectral density functions of wave surface elevations is the JONSWAP spectrum [22]. By introducing $\hat{\omega} = (\omega/\omega_0)$ where ω_0 is the peak spectral frequency of the wave surface elevations, the JONSWAP spectrum can be written in a dimensionless form:

$$\hat{S}_{\eta\eta}(\hat{\omega}) = \frac{S_{\eta\eta}(\omega)}{S_{\eta\eta}(\omega_0)} = \exp(1.25)\hat{\omega}^{-5}\exp(-1.25\hat{\omega}^{-4})\gamma^{\mu-1} \tag{2}$$

where ω_0 is a function of wind velocity and fetch length, γ is the sharpness magnification factor, $\mu = \exp[-(1/2\sigma^2)(1-\hat{\omega})^2]$ with $\sigma = 0.07$ for $\hat{\omega} \leqslant 1$ and $\sigma = 0.09$ for $\hat{\omega} > 1$. If γ is set equal to unity, the JONSWAP spectrum reduces to the other commonly used spectrum, the Pierson–Moskovitz spectrum. In Reference [28], the non-dimensional form of the JONSWAP spectrum was modelled by employing a cascade of two linear second-order filters as

$$\hat{S}_{\eta\eta}(\hat{\omega}) \approx \hat{S}_A = \frac{G\hat{\omega}^4}{[(\hat{\omega}^2 - k_1)^2 + (c_1\hat{\omega})^2][(\hat{\omega}^2 - k_2)^2 + (c_2\hat{\omega})^2]} \tag{3}$$

where the parameters G, k_1, k_2, c_1 and c_2 are determined by a least-squares algorithm [28]. Note that Equation (3) represents a single-input, single-output (SISO) system. This form of the JONSWAP spectrum is utilized in this study because it can be conveniently expressed by a state-space model.

The spectral density function of the horizontal water-particle velocities at any water level z is related to the spectral density function of wave surface elevations via [22, 29, 30]

$$S_{vv}(\omega, z) = |H_{v\eta}(\mathrm{j}\omega, z)|^2 S_{\eta\eta}(\omega). \tag{4}$$

Following the linear wave theory, the magnitude of the transfer function from wave surface elevation to horizontal water-particle velocities is

$$|H_{v\eta}(\mathrm{j}\omega,z)|^2 = \omega^2\Lambda(\omega,z)(1+\cos\kappa b(z))S_{\eta\eta}(\omega)$$
$$\Lambda(\omega,z) = \frac{\cosh^2(\kappa z)}{\sinh^2(\kappa d)} \tag{5}$$

where $\mathrm{j}=\sqrt{-1}$, $\kappa=\omega^2/g$ is the wave number, g is the acceleration due to gravity, $b(z)$ is the horizontal distance between the two legs of the platform in the direction of wave propagation at level z and d is the water depth.

The relationship between the spectral density function of the wave forces per unit depth of the platform and the spectral density function of the horizontal water-particle velocities can be obtained from the linear wave theory [22, 30]. The cross-spectral density function of the wave forces per unit depth of the platform between water levels z_m and z_n is

$$S_{q_m,q_n}(\omega,z_m,z_n) = S_i(\omega,z_m,z_n) + S_{\mathrm{I}}(\omega,z_m,z_n) + S_{\mathrm{II}}(\omega,z_m,z_n) + S_{\mathrm{III}}(\omega,z_m,z_n) \tag{6}$$

where the spectral density function of the inertia force is

$$S_i(\omega,z_m,z_n) = k_{\mathrm{I}}(z_m)k_{\mathrm{I}}(z_n)S_{a_ma_n}(\omega), \tag{7}$$

the spectral density function of the linear part of the wave drag force is

$$S_{\mathrm{I}}(\omega,z_m,z_n) = k_D(z_m)k_D(z_n)B(\gamma_{\mathrm{c}}(z_m))B(\gamma_{\mathrm{c}}(z_n))\sigma_{v_m}\sigma_{v_n}S_{v_mv_n}(\omega) \tag{8}$$

the spectral density function of the non-linear wave force can be expressed in terms of a quadratic and cubic representation, $S_{\mathrm{II}}(\omega)$ and $S_{\mathrm{III}}(\omega)$, given below

$$S_{\mathrm{II}}(\omega,z_m,z_n) = 2k_{\mathrm{D}}(z_m)k_{\mathrm{D}}(z_n)\Phi(\gamma_{\mathrm{c}}(z_m))\Phi(\gamma_{\mathrm{c}}(z_n))S^{*2}_{v_mv_n}(\omega) \tag{9}$$

$$S_{\mathrm{III}}(\omega,z_m,z_n) = \frac{8}{3}\frac{k_{\mathrm{D}}(z_m)k_{\mathrm{D}}(z_n)}{\sigma_{v_m}\sigma_{v_n}}\phi(\gamma_{\mathrm{c}}(z_m))\phi(\gamma_{\mathrm{c}}(z_n))S^{*3}_{v_mv_n}(\omega) \tag{10}$$

$$k_{\mathrm{I}}(z) = \frac{\pi}{4}\rho C_{\mathrm{M}}D^2(z)$$
$$k_{\mathrm{D}}(z) = \tfrac{1}{2}\rho C_{\mathrm{D}}D(z)$$
$$B(\gamma_{\mathrm{c}}(z)) = 2\gamma_{\mathrm{c}}(z)\Phi(\gamma_{\mathrm{c}}(z)) + 4\phi(\gamma_{\mathrm{c}}(z))$$
$$\gamma_{\mathrm{c}}(z) = \frac{U_{\mathrm{c}}}{\sigma_u(z)}$$
$$\Phi(\gamma_{\mathrm{c}}(z)) = 2\int_0^{\gamma_{\mathrm{c}}(z)}\phi(t)\,\mathrm{d}t$$
$$\phi(\gamma_{\mathrm{c}}(z)) = \frac{1}{\sqrt{2\pi}}\exp-\frac{\gamma_{\mathrm{c}}^2(z)}{2}$$

and the spectrum of wave particle acceleration is

$$S_{a_ma_n}(\omega) = \omega^2 S_{v_mv_n}(\omega) \tag{11}$$

where ρ is the density of the water, C_D is the drag coefficient, C_M is the inertia coefficient, $D(z)$ is the characteristic diameter of the platform leg at water level z, U_c is the uniform water current, $\sigma_u(z)$ is the standard deviation of the wave particle velocity at water level z, σ_{v_m} is the standard deviation of the horizontal wave velocities at water level z_m and the convolution S^{*n} is defined as

$$S^{*n}(\omega) \triangleq \int_{-\infty}^{\infty} S(g)^{*(n-1)} S(\omega - g)\,\mathrm{d}g \tag{12}$$

It is the contributions of $S_{II}(\omega)$ and $S_{III}(\omega)$ which result in energy at frequencies both inside and outside the range of frequencies associated with the base process. The square and cube in the time domain are associated with the respective convolution in the frequency domain by the Fourier transform relationship between the two operations. The second-order convolution places energy at sums and differences frequencies representatives of the base process. The third-order convolution spreads energy about the central frequency of the base process at its third harmonic.

The spectral distortion effect of non-linearities is important because, via this mechanism, energy can creep into frequency ranges which are critical to a structural system being acted upon. If this effect is ignored, significant structural response energy may also go by the wayside, leading to non-conservative response estimates.

Notice that for a multi-input, multi-output (MIMO) wave force model, $\sigma_{v_m}\sigma_{v_n}$ is an element of the covariance matrix of the horizontal water-particle velocities. In the presence of currents, the loading non-linearity is statistically asymmetric and the problem can essentially be treated with a quadratic representation. In the absence of current, i.e. a statistically symmetric non-linear case, the quadratic term drops out and the cubic term $S_{III}()$ becomes more significant. In other cases, both terms contribute depending on the current amplitude [31].

Filter for S_I. In modelling the wave forces, the spectral density matrix factorization approach will be used [32]. In this approach, a random process with a spectral density matrix $S(\omega)$ is modelled as the output of a filter with a unit intensity white noise process as an input. In the Laplace domain (by substituting s for $j\omega$ or $-s^2$ for ω^2), this spectral density matrix is factorized as

$$S(s) = H(-s)H^*(s) \tag{13}$$

where H^* is the transpose of the complex conjugate of H. Using the definition of the spectral density function, it can be shown that if the input of $H(s)$ is a unit intensity white noise, then the output of $H(s)$ will have a spectral density of $S(s)$. $H(s)$ is then expressed in the state-space format for the control design.

In the jacket-type offshore platform model used in this study, the wave forces will be acting at five levels. Therefore, a wave force model must be constructed that has one input, i.e. a unit intensity white noise, and five outputs, i.e. the wave forces on the platform at different depths. To simplify the procedure, this modelling will be done in three steps. The first step is to model the wave surface elevations. This is accomplished using a SISO model obtained from Equation (13) with a unit intensity white-noise process as an input and wave surface elevations as output. The second step is to model the transfer function from the wave surface elevation to the horizontal wave velocity. Five SISO models with wave elevations as input and horizontal water-particle velocities at five levels of the platform legs as output are obtained

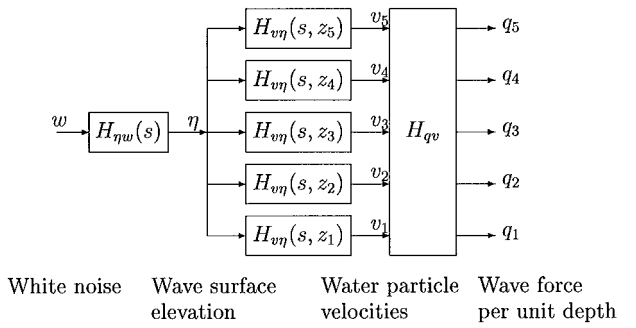

Figure 1. A full model of wave forces on offshore platforms.

separately. The third step is to use the results of the first two steps to obtain the final model. Note that the second step can be done in the same manner as the first step because

$$|H_{v\eta}(\mathrm{j}w)|^2 = H_{v\eta}(-\mathrm{j}w)H^*_{v\eta}(\mathrm{j}w) \tag{14}$$

which is the same form as Equation (13). The third step, which transfers the five horizontal water-particle velocities into five wave forces on the legs of the platform, involves only constants.

The modelling of $H_{\eta w}$, the transfer function between the input white noise and the wave height fluctuation, in the first step and of $H_{v\eta}$ in the second step is equivalent to the modelling of the filter for S_{vv}. By Equation (13),

$$S_{vv}(s) = H_{vw}(-s)H^*_{vw}(s) \tag{15}$$

By substituting $H_{vw}(s) = H_{v\eta}(s)H_{\eta w}(s)$ into Equation (15), the following is obtained:

$$S_{vv}(s) = H_{v\eta}(-s)H_{\eta w}(-s)H^*_{v\eta}(s)H^*_{\eta w}(s) \tag{16}$$

The resulting full model that transfers a unit intensity white-noise process into wave forces on the platform is shown in Figure 1. In this figure, w is the unit intensity white-noise process, η is the wave surface elevations, v is the horizontal water-particle velocities and q is the wave forces per unit depth of the platform.

Filters for S_i, S_{II}, and S_{III}. The filters for S_i, S_{II} and S_{III} can be obtained in a similar manner as the filter for S_{I}. For the S_i filter, the power spectral density function of the water-particle acceleration $S_{a_m a_n}$ is needed. This function can be obtained from $S_{v_m v_n}$ by Equation (11), which is the following in the Laplace domain:

$$S_{a_m a_n}(s) = -s^2 S_{v_m v_n}(s) \tag{17}$$

The filter for $S_{a_m a_n}$ can then be obtained using the same procedure as the first step in obtaining the filter for $S_{v_m v_n}$. From that, the filter for S_i can be obtained following the second and third steps in obtaining S_{I}. For the filters of S_{II} and S_{III}, the power spectral density functions $S^{*2}_{v_m v_n}$ and $S^{*3}_{v_m v_n}$ are needed. These functions can be numerically obtained from the convolution of $S_{v_m v_n}$ as described in Equation (12). The results are pairs of numbers describing $S^{*2}_{v_m v_n}$ and $S^{*3}_{v_m v_n}$.

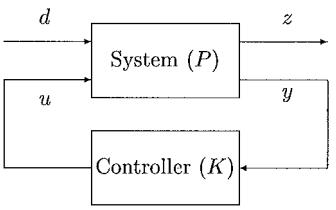

Figure 2. Basic structural control system.

By some curve-fit processes, these numerical results are then presented as ratios of polynomials which can be factorized as in Equation (13). From these ratios of polynomials, the filters for $S^{*2}_{v_m v_n}$ and $S^{*3}_{v_m v_n}$ are obtained. Once these filters are obtained, the procedures for obtaining the S_{II} and S_{III} filters are straightforward.

Frequency domain control

Using a block diagram description, the structural control problem can be depicted as in Figure 2, where y is the measured output vector, z is the regulated output vector, u is the control input vector and d is the exogenous input vector. The regulated output vector z may consist of any combination of states of the system and components of the control input vector u. By appropriately choosing elements of z, different control design objectives can be included in the problem formulation. Weighting functions can be added to elements of z to determine the frequency range where each element of z is to be minimized. The 'system' in Figure 2 can then contain the structure and the filters and weighting functions in the frequency domain.

The task here is to design a stabilizing controller in such a way that the norm or 'size' of the transfer function from disturbance d to regulated output z is minimized [15]. The control design method which minimizes this H_2 norm is termed the H_2 control. The freedom of the control designer to choose elements of z and frequency dependent weighting functions makes this approach very flexible.

Let the 'system' in Figure 2 be denoted by P and the 'controller' by K. Partitioning P into its components,

$$P = \begin{bmatrix} P_{zd} & P_{zu} \\ P_{yd} & P_{yu} \end{bmatrix} \tag{18}$$

It is shown that

$$y = P_{yd}d + P_{yu}u = P_{yd}d + P_{yu}Ky \tag{19}$$

and

$$z = P_{zd}d + P_{zu}u \tag{20}$$

Note that in Equation (18), a matrix with square brackets is used instead of a matrix with parentheses. This notation is used to emphasize that the elements of the matrix are not constant matrices, but transfer functions.

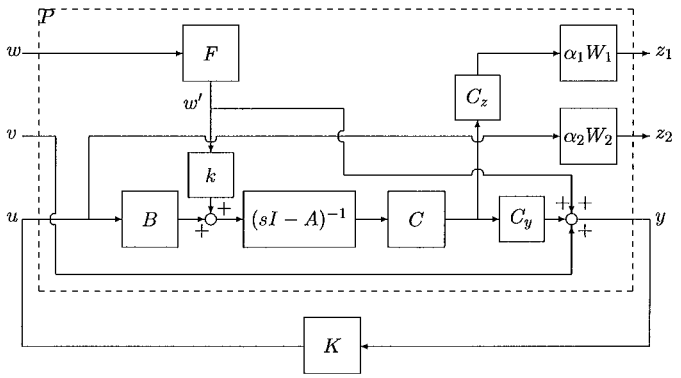

Figure 3. A control problem for offshore platform under wave loading.

By rearranging Equation (19) and substituting it into Equation (20), the following is obtained:

$$z = [P_{zd} + P_{zu}K(I - P_{yu}K)^{-1}P_{yd}]d$$

or

$$z = H_{zd}d \tag{21}$$

where

$$H_{zd} = P_{zd} + P_{zu}K(I - P_{yu}K)^{-1}P_{yd} \tag{22}$$

H_{zd} is the transfer function from d to z that needs to be minimized. One possible block diagram set-up for P is depicted in Figure 3.

In this figure, A, B and C are matrices that form the state-space representation of the Equations of motion of the platform. The block F represents the wave force model. C_z and C_y are matrices needed to extract parts of the system output to form regulated and measured output vectors. The input of F is a vector of unit-intensity white-noise processes, w. The output of F is a vector of wave forces, w'. The control force u and the wave forces w' generally enter the system differently. For example, the control force comes into the system via the active control device as indicated by the matrix B, while wave forces produce loadings on every lumped mass of the platform. The external excitation d consists of two elements: w and v, or

$$d = \begin{pmatrix} w \\ v \end{pmatrix} \tag{23}$$

where w is a white-noise input vector to the wave force model filter and v is the measurement noise. The regulated output z consists of z_1 and z_2, i.e.

$$z = \begin{pmatrix} z_1 \\ z_2 \end{pmatrix} \tag{24}$$

where z_1 is the weighted structural response and z_2 is the weighted control force.

The objective of the control design is to determine a controller K such that a weighted norm of the transfer function from d to z is minimized. With this set-up, the matrix P expressed in the form of Equation (18) is given by

$$P = \begin{bmatrix} P_{z_1 w} & P_{z_1 v} & P_{z_1 u} \\ P_{z_2 w} & P_{z_2 v} & P_{z_2 u} \\ P_{yw} & P_{yv} & P_{yu} \end{bmatrix} = \begin{bmatrix} \alpha_1 W_1 C_z G' k & 0 & \alpha_1 W_1 C_z G \\ 0 & 0 & \alpha_2 W_2 \\ C_y G' k + F & I & C_y G \end{bmatrix} \tag{25}$$

In Figure 3 and Equation (25), W_1 and W_2 are frequency-dependent weighting functions, α_1 and α_2 are scalar multipliers for W_1 and W_2, respectively and k is a scalar which expresses a preference in minimizing the transfer function from d to z versus minimizing the transfer function from v to z. If k is taken as a large value, then the effect of measurement noise is neglected in the control design. The transfer functions G and G' are defined as

$$G \triangleq C(sI - A)^{-1}B \tag{26}$$

and

$$G' \triangleq C(sI - A)^{-1}F \tag{27}$$

From Equation (25), the transfer function to be minimized, H_{zd}, can be computed by Equation (22). The result is

$$H_{zd} = \begin{bmatrix} H_{z_1 w} & H_{z_1 v} \\ H_{z_2 w} & H_{z_2 v} \end{bmatrix} \tag{28}$$

where

$$\begin{aligned} H_{zd}(11) &= \alpha_1 W_1 (C_z G' k + C_z GK(I - C_y GK)^{-1} C_y G' k) \\ H_{zd}(12) &= \alpha_1 W_1 C_z GK(I - C_y GK)^{-1} \\ H_{zd}(21) &= \alpha_2 W_2 K(I - C_y GK)^{-1}(C_y G' k + F) \\ H_{zd}(22) &= \alpha_2 W_2 K(I - C_y GK)^{-1} \end{aligned}$$

Increasing $\alpha_1 W_1$ in the frequency range while choosing a large value of k causes the transfer function from the white-noise excitation vector w to the weighted structural response z_1 to be minimized more. This will help improve the performance of the system at those frequencies. Increasing α_2 in the frequency range while choosing a large value of k also causes the transfer function from the white-noise excitation w to the weighted control force z_2 to be minimized more. This will help limit the control forces. Increasing one of the weightings in a frequency range decreases the importance of the other weighting in that frequency range. Therefore, one is faced with a tradeoff between different design objectives. The H_2 control strategy searches for a stabilizing controller while minimizing the H_2 norm of H_{zd}, $\|H_{zd}\|_2$. The H_2 solution procedure is given in Appendix A.

EXAMPLE

Modelling of the wave force spectrum

In the first part of this example, the wave force spectrum is modelled. The sea state is defined by the JONSWAP wave spectrum. The peak spectral frequency is $\omega_0 = 0.35$ rad/s, which corresponds to a period of 18 s. The sharpness magnification factor is $\gamma = 3.78$.

The modelling of the $S_i, S_{\mathrm{I}}, S_{\mathrm{II}}$, and S_{III} filters will be described separately. These filters will then be added together to obtain the total wave force filter.

Filter of S_{I}

The following parameters are used in Equation (3): $G=0.47,\ k_1=1,\ k_2=4,\ c_1=0.15$ and $c_2=3.5$ [28]. A significant wave height of 15 m was obtained by setting $G=0.47$. The numerator and denominator of the spectral density function can be treated separately because this process involves a SISO system. In the Laplace domain, the numerator of $\hat{S}_A$ in Equation (3) is

$$\frac{G}{\omega_0^4}s^4 = 3331.9s^4 \tag{29}$$

Let the model filter for $\hat{S}_A$ be denoted as $H_{\eta w}$. The numerator of the filter $H_{\eta w}$ is then simply

$$\frac{\sqrt{G}}{\omega_0^2}s^2 = 57.723s^2 \tag{30}$$

The denominator of $\hat{S}_A$ is

$$\begin{aligned}&\left[\left(\frac{-1}{\omega_0^2}s^2 - k_1\right)^2 + \left(\frac{-\mathrm{j}c_1}{\omega_0}s\right)^2\right]\left[\left(\frac{-1}{\omega_0^2}s^2 - k_2\right)^2 + \left(\frac{-\mathrm{j}c_2}{\omega_0}s\right)^2\right]\\ &= 4440.7(s^2 - 1.2250s + 0.4900)(s^2 + 1.2250s + 0.4900)\\ &\quad (s^2 - 0.0525s + 0.1225)(s^2 + 0.0525s + 0.1225)\end{aligned} \tag{31}$$

The denominator of the filter $H_{\eta w}$ is obtained by choosing the stable parts from the pairs in Equation (31), i.e. the denominator of the filter $H_{\eta w}$ is

$$66.639(s^2 + 1.2250s + 0.4900)(s^2 + 0.0525s + 0.1225) \tag{32}$$

Hence

$$H_{\eta w}(s) = \frac{57.723s^2}{66.639(s^2 + 1.2250s + 0.4900)(s^2 + 0.0525s + 0.1225)} \tag{33}$$

It can be readily shown that

$$H_{\eta w}(-s)H_{\eta w}^*(s) = H_{\eta w}(-s)H_{\eta w}(s) = \hat{S}_A(s) \tag{34}$$

Recall from Equation (5) that the magnitude of the transfer function from wave surface elevations to horizontal water-particle velocities is

$$|H_{v\eta}(\mathrm{j}\omega, z)|^2 = \omega^2\Lambda(\omega, z)(1 + \cos\kappa b(z)) \tag{35}$$

with

$$\Lambda(\omega, z) = \frac{\cosh^2(\kappa z)}{\sinh^2(\kappa d)} = \frac{1 + \frac{1}{2}(\kappa z)^2 + \frac{1}{24}(\kappa z)^4 + \frac{1}{720}(\kappa z)^6 + \cdots}{1 + \frac{1}{6}(\kappa d)^3 + \frac{1}{120}(\kappa d)^5 + \frac{1}{5040}(\kappa d)^7 + \cdots} \tag{36}$$

Also

$$(1+\cos\kappa b)=2-\tfrac{1}{2}(\kappa b)^2+\tfrac{1}{24}(\kappa b)^4-\tfrac{1}{720}(\kappa b)^6+\cdots \tag{37}$$

Let the numerator of $|H_{v\eta}|^2$ be denoted by N_H and its denominator by D_H. Substituting $\kappa=\omega^2/g, \omega^2=-s^2$, and truncating up to the sixth power of s, we obtain

$$N_H(s,z)=\frac{2z^2-b^2}{2g^2}s^6+2s^2 \tag{38}$$

and

$$D_H(s)=\frac{d^3}{6g^3}s^6-1 \tag{39}$$

Now, using the same procedure as in the first step, $N_H(s,z)$ and $D_H(s)$ can be easily factorized to obtain the numerator and denominator of the model filter $H_{v\eta}(s,z)$.

The third step is to 'factorize' a constant matrix S with individual element $(8/\pi)k_D(z_m)k_D(z_n)\sigma_{v_m}\sigma_{v_n}$ and to connect the result to $H_{v\eta}$ and $H_{\eta w}$. Note that $\sigma_{v_m}\sigma_{v_n}$ is an element of the covariance matrix of the horizontal water-particle velocities. The 'factorization' here is to find a matrix H_{qv} such that

$$S=H_{qv}H_{qv}^{\mathrm{T}} \tag{40}$$

which simplifies into

$$H_{qv}=S^{1/2} \tag{41}$$

where H_{qv} is a constant matrix of real numbers due to the fact that S is symmetric. This operation can be done using various available matrix decomposition algorithms.

Filter of S_i

The filter of the wave particle acceleration spectrum is

$$H_a(s)=s\frac{N_{H_{\eta w}}(s)}{D_{H_{\eta w}}(s)}\frac{N_{H_{v\eta}}(s)}{D_{H_{v\eta}}(s)} \tag{42}$$

This wave particle acceleration filter will then be used to calculate S_i in Equation (7) following the three steps described above.

Filter of S_{II}

The second-order convolution of the wave-particle velocity spectrum is calculated from the first-order convolution wave particle velocity spectrum [Equation (9)]. This spectrum is curve-fitted by the following function:

$$S_u^{*2}(s)=\frac{N_{S_u^{*2}}(s)}{D_{S_u^{*2}}(s)} \tag{43}$$

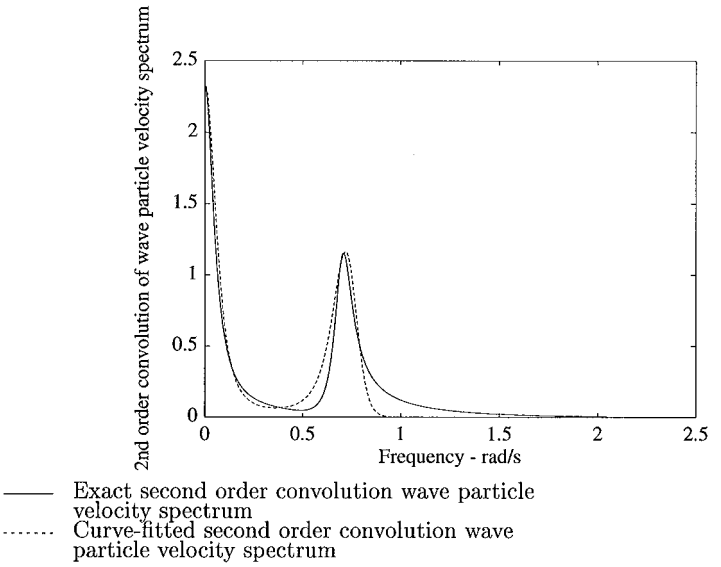

Figure 4. Second-order convolution wave particle velocity spectra.

where $N_{S_u^{*2}}(s) = 3.9700E{-}05$ and

$$D_{S_u^{*2}}(s) = s^{24} - (2.1185E+00)s^{22} - (9.1675E+00)s^{20} + (3.2935E{-}01)s^{18} + (3.3090E+01)s^{16} + (5.8484E+01)s^{14} + (5.2266E+01)s^{12} + (2.7996E+01)s^{10} + (9.1206E+00)s^{8} + (1.6584E+00)s^{6} + (1.1996E{-}01)s^{4} - (2.9456E{-}03)s^{2} + (1.5707E-05) \quad (44)$$

Both the exact and curve-fitted spectra are plotted in Figure 4, which exhibits a good match of the overall frequency distribution of the spectral amplitude.

Based on the spectrum in Equation (43), the second-order convolution wave particle velocity filter is obtained as

$$F_{u\mathrm{II}}(s) = \frac{N_{F_{u\mathrm{II}}}(s)}{D_{F_{u\mathrm{II}}}(s)} \quad (45)$$

where $N_{F_{u\mathrm{II}}}(s) = 6.3008E{-}03$ and

$$D_{F_{u\mathrm{II}}}(s) = s^{12} + (5.0108E+00)s^{11} + (1.1495E+01)s^{10} + (1.8849E+01)s^{9} + (2.3803E+01)s^{8} + (2.2850E+01)s^{7} + (1.8701E+01)s^{6} + (1.1404E+01)s^{5} + (6.1276E+00)s^{4} + (2.2013E+00)s^{3} + (6.8929E{-}01)s^{2} + (9.1702E{-}02)s + (3.9633E{-}03) \quad (46)$$

This second-order convolution wave particle velocity filter will then be used to calculate S_{II} by Equation (9).

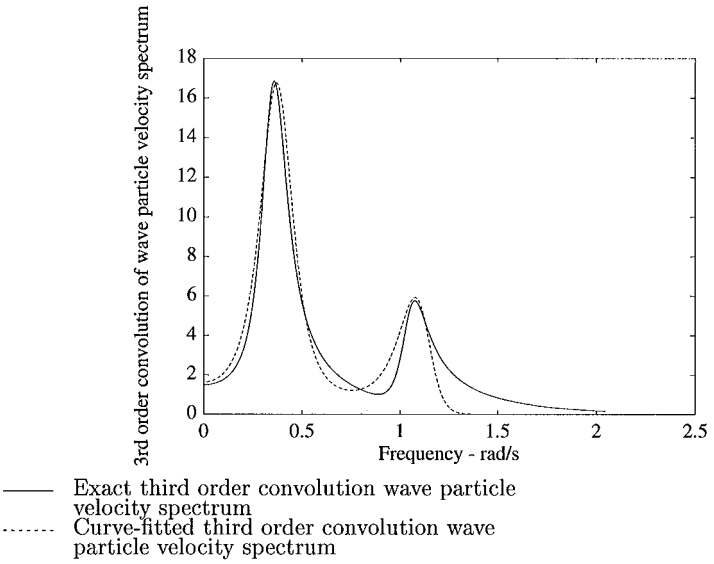

Figure 5. Third-order convolution wave particle velocity spectra.

Filter of S_{III}

The third-order convolution of wave particle velocity spectrum is calculated by Equation (10) from the first- and second-order convolution wave particle velocity spectra. This spectrum is curve-fitted by functions that can be factorized according to Equation (13). For example, the third-order convolution of wave particle velocity spectrum for the wave with a period of 18 s that enters the platform at its fifth lumped mass is curve-fitted by a function

$$S_u^{*3}(s) = \frac{N_{S_u^{*3}}(s)}{D_{S_u^{*3}}(s)} \tag{47}$$

with $N_{S_u^{*3}}(s) = 0.01$ and

$$\begin{aligned} D_{S_u^{*3}}(s) = {} & s^{24} + 1.0476 \times 10^1 s^{22} + 4.9357 \times 10^1 s^{20} + 1.3717 \times 10^2 s^{18} + 2.4798 \times 10^2 s^{16} \\ & + 3.0324 \times 10^2 s^{14} + 2.5286 \times 10^2 s^{12} + 1.4173 \times 10^2 s^{10} + 5.1760 \times 10^1 s^8 \\ & + 1.1923 \times 10^1 s^6 + 1.7372 s^4 + 1.4821 \times 10^{-1} s^2 + 6.1326 \times 10^{-3} \end{aligned} \tag{48}$$

Both the exact and the curve-fitted spectra are plotted in Figure 5.

Based on the spectrum in Equation (47), the third-order convolution wave particle velocity filter is obtained as

$$F_{u\mathrm{III}}(s) = \frac{N_{F_{u\mathrm{III}}}(s)}{D_{F_{u\mathrm{III}}}(s)} \tag{49}$$

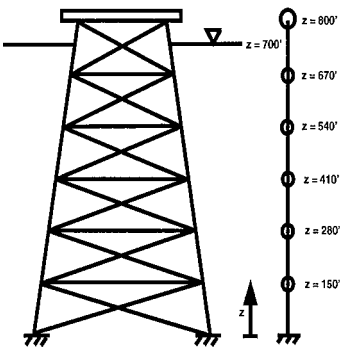

Figure 6. Elevation of jacket-type offshore platform A used in numerical example.

where $N_{F_{u\mathrm{III}}}(s) = 2.1794 \times 10^{-2}$ and

$$D_{F_{u\mathrm{III}}}(s) = s^{12} + 1.9656s^{11} + 7.1982s^{10} + 9.7126s^{9} + 1.8081 \times 10^{1}s^{8} + 1.7157 \times 10^{1}s^{7} + 2.0043 \times 10^{1}s^{6} + 1.3004 \times 10^{1}s^{5} + 9.7087s^{4} + 3.9011s^{3} + 1.6588s^{2} + 3.2358 \times 10^{-1}s + 7.0769 \times 10^{-2} \quad (50)$$

This third-order convolution wave particle velocity filter will then be used to calculate S_{III} in Equation (10).

NUMERICAL ANALYSIS OF OFFSHORE PLATFORM CONTROL

Platform characteristics

In the second part of this example, the motion of two jacket-type offshore platforms is controlled utilizing both passive and active control strategies. The passive control device studied is the tuned mass damper. The active devices analysed here include the active mass damper, the active tendon mechanism and the propeller thruster. Each platform is individually modelled as six lumped masses, as shown in Figure 6. For each platform, five of these masses are located below the mean sea level.

Platform A. For the first platform, the depth of the sea is set at 700 ft. The lumped masses are $2 \times 10^5, 1.8 \times 10^5, 1.6 \times 10^5, 1.4 \times 10^5, 1.2 \times 10^5$ and 1.0×10^6 slugs, located at $z = 150, 280, 410, 540, 670$ and 800 ft above the sea bed, respectively. The distances between the legs of the platforms below the mean sea level at the locations of the lumped masses are $b(z) = 165, 148.75, 132.5, 116.25$ and 100 ft, respectively. The corresponding equivalent characteristic diameters of the legs are $D(z) = 45, 40, 35, 30$ and 25 ft, respectively. The equivalent characteristic diameter represents the total projected diameter of the platform legs at given elevations. The wave phase effect that results from the spatial separation between legs is accounted in the formulation [Equation (5)].

The first six natural frequencies of this platform are 0.2, 0.98171, 1.9527, 2.7209, 3.2802 and 3.8471 cycles/sec (Hz), respectively. The corresponding modal damping ratios are 0.02, 0.049704, 0.0866, 0.11579, 0.13705 and 0.15859, respectively.

Platform B. For the second platform, the depth of the sea is set at 1150 ft. The lumped masses are the same as those used for Platform A (i.e. 2×10^5, 1.8×10^5, 1.6×10^5, 1.4×10^5, 1.2×10^5 and 1.0×10^6 slugs). However, these masses are now located at $z = 200, 400, 600, 800, 1000$ and 1250 ft above the sea bed, respectively. The distances between the legs of the platforms below the mean sea level at the locations of the lumped masses are $b(z) = 226, 202, 178, 154$ and 130 ft, respectively.

The first six natural frequencies of Platform B are 0.16692, 0.81933, 1.6297, 2.2709, 2.7376 and 32.108, respectively. The corresponding modal damping ratios are 0.02, 0.049704, 0.0866, 0.11579, 0.13705 and 0.15859, respectively.

Sea states

Different sea states are applied for this study. The sea states are defined by the JONSWAP wave spectrum, using a sharpness magnification factor $\gamma = 3.78$ and periods of 18, 14, 10 and 6 sec, respectively. It is noteworthy that the 18 sec dominant wave spectrum has considerable energy at or around the first natural periods of the two platforms studied here. This may result in large deck displacements even though the platform natural periods are removed from the dominant wave period in a sea state. Furthermore, higher-order loading component may add to the response at the platform natural period.

NUMERICAL RESULTS

The block diagram description for this control problem is given in Figure 3. In this figure, the matrix C_z is such that the regulated output z_1 is the weighted displacement of the platform deck and C_y is such that the measured output y is the accelerations of all the lumped masses of the platform. The numerical results obtained using various control set-ups on platform A are given in Tables I–IV. The numerical results obtained using various control set-ups on platform B are given in Tables V–VIII. In these tables, σ_{d_6} is the standard deviation of the displacement of the top mass in cm, and $\sigma_{d_{MD}}$ is the standard deviation of the displacement of the mass damper. The last entry in these tables, σ_u, represents the standard deviations of the control force generated by the active control device. Various cases examined in these tables are listed below.

Case I represents the platform with no external control device. Case II represents the platform with a TMD installed on the platform deck. The design of the optimum TMD is based on the design formulae in Reference [33]. The properties of the TMD are: mass = 172 t (1 per cent of the generalized mass associated with the first mode of the platform), stiffness = 268 kN/m and damping coefficient = 20 t/s. The eigenfrequency of the damper is 0.199 Hz, which is 99.3 per cent of the first natural frequency of the platform.

Case III represents the platform with an AMD installed (1 per cent of the generalized mass associated with the first mode of the platform). The goal of structural control is to reduce the structural response in the frequency range where the structure is sensitive to disturbance, i.e., at

Table I. Standard deviations of displacements and control forces: platform A, wave period = 18 s.

Case	σ_{d_6} (cm) (deck)	% reduction	$\sigma_{d_{MD}}$ (cm) (damper)	σ_u (kN) (control force)
I	1.9236E1	—	—	—
II	1.7151E1	10.8	7.3883E1	—
III	1.4345E1	25.4	2.3101E2	3.2291E2
IV	1.3507E1	29.8	—	3.9293E3
V	1.4000E1	27.2	—	7.6260E2
VI	1.3685E1	28.9	6.0375E1	3.8310E1
VII	1.3637E1	29.1	5.9009E1	9.2715E2

Table II. Standard deviations of displacements and control forces: platform A, wave period = 14 s.

Case	σ_{d_6} (cm) (deck)	% reduction	$\sigma_{d_{MD}}$ (cm) (damper)	σ_u (kN) (control force)
I	1.3643E1	—	—	—
II	1.0133E1	25.7	5.9812E1	—
III	7.1899E0	47.3	1.4431E2	1.8482E2
IV	7.1896E0	47.3	—	1.7870E3
V	7.3082E0	46.4	—	3.5478E2
VI	7.2164E0	47.1	4.5818E1	1.6174E3
VII	7.1780E0	47.4	4.4596E1	3.7588E2

Table III. Standard deviations of displacements and control forces: platform A, wave period = 10 s.

Case	σ_{d_6} (cm) (deck)	% reduction	$\sigma_{d_{MD}}$ (cm) (damper)	σ_u (kN) (control force)
I	7.6417E0	—	—	—
II	5.6128E0	26.6	3.5066E1	—
III	3.8773E0	49.3	8.4810E1	1.0482E2
IV	3.9415E0	48.4	—	6.8261E2
V	3.9889E0	47.8	—	1.3913E2
VI	3.9123E0	48.8	3.0947E1	6.5825E2
VII	3.8965E0	49.0	2.8710E1	1.3641E2

low frequencies. At high frequencies where the structure is often not sensitive to disturbance, the control should "roll off" or lower because it is not effective. Therefore, to minimize the structural response, a weighting function which has a large magnitude at low frequencies and rolls off at high frequencies is needed. One class of functions that satisfies these requirements is in the form of $(a/(s+a))^n$, $n = 1, 2, 3, \ldots$. Here, a is termed the "corner frequency", i.e. the frequency where the function "starts" to roll-off. The slope of the roll-off depends on n: a

Table IV. Standard deviations of displacements and control forces: platform A, wave period = 6 s.

Case	σ_{d_6} (cm) (deck)	% reduction	$\sigma_{d_{MD}}$ (cm) (damper)	σ_u (kN) (control force)
I	6.4129E0	—	—	—
II	4.7863E0	25.4	3.1443E1	—
III	2.0849E0	67.5	9.1357E1	9.3222E1
IV	2.0653E0	67.8	—	8.1844E2
V	2.1355E0	66.7	—	1.7679E2
VI	2.0532E0	68.0	1.7294E1	7.6264E2
VII	1.9528E0	69.5	1.6447E1	1.8552E2

Table V. Standard deviations of displacements and control forces: platform B, wave period = 18 s.

Case	σ_{d_6} (cm) (deck)	% reduction	$\sigma_{d_{MD}}$ (cm) (damper)	σ_u (kN) (control force)
I	5.9848E1	—	—	—
II	4.1441E1	30.8	2.4776E2	—
III	2.7636E1	53.8	8.1167E2	1.0496E3
IV	2.7332E1	54.3	—	6.8849E3
V	2.6653E1	55.5	—	1.8602E3
VI	2.7070E1	54.8	1.7053E2	6.6043E3
VII	2.6541E1	55.7	1.0340E2	1.3607E3

Table VI. Standard deviations of displacements and control forces: platform B, wave period = 14 s.

Case	σ_{d_6} (cm) (deck)	% reduction	$\sigma_{d_{MD}}$ (cm) (damper)	σ_u (kN) (control force)
I	3.0299E1	—	—	—
II	2.2761E1	24.9	1.3083E2	—
III	1.5079E1	50.2	5.1214E2	6.4906E2
IV	1.4540E1	52.0	—	2.9217E3
V	1.4294E1	52.8	—	6.9490E2
VI	1.4695E1	51.5	8.8036E1	2.6991E3
VII	1.4791E1	51.2	8.6345E1	6.7750E2

larger n yields a steeper slope. For this example, the weighting function is

$$W_1 = \frac{a}{s+a} \tag{51}$$

The corner frequency $a = 4$ rad/s is used throughout these numerical studies. To minimize control forces, a weighting function which has a small magnitude at low frequencies and

Table VII. Standard deviations of displacements and control forces: platform B, wave period = 10 s.

Case	σ_{d_6} (cm) (deck)	% reduction	$\sigma_{d_{MD}}$ (cm) (damper)	σ_u (kN) (control force)
I	2.1724E1	—	—	—
II	1.5923E1	26.7	9.7026E1	—
III	8.4441E0	61.1	3.8494E2	4.3085E2
IV	8.4310E0	61.2	—	2.3465E3
V	8.4631E0	61.0	—	5.5603E2
VI	8.4538E0	61.1	5.9518E1	1.9069E3
VII	8.4989E0	60.9	5.8387E1	4.5776E2

Table VIII. Standard deviations of displacements and control forces: platform B, wave period = 6 s.

Case	σ_{d_6} (cm) (deck)	% reduction	$\sigma_{d_{MD}}$ (cm) (damper)	σ_u (kN) (control force)
I	2.9250E1	—	—	—
II	1.8144E1	38.0	1.3711E2	—
III	3.2687E0	88.8	2.8549E2	1.6477E2
IV	3.2483E0	88.9	—	2.5242E3
V	3.2407E0	88.9	—	5.8984E2
VI	3.2432E0	88.9	5.1808E1	2.4627E3
VII	3.2204E0	89.0	5.1746E1	5.4947E2

increases at high frequencies is needed. For this example, the following is used:

$$W_2 = \frac{s + 0.1}{1 \times 10^{-6} s + 0.1} \tag{52}$$

These weighting functions are plotted in Figure 7.

Case IV represents the platform with a tendon mechanism located between its fifth and sixth lumped masses. The active tendon system consists of a diagonal set of tendons/pulley with an actuator which transmits its force by altering tension in tendons, thus the system characteristics.

Case V represents the platform with a propeller thruster located on its fifth lumped mass. Case VI represents the platform with a combination of a TMD and a tendon mechanism located between its fifth and sixth lumped masses. Case VII represents the platform with a combination of a TMD and a propeller thruster located on its fifth lumped mass.

The above tables show that the response of the platform is reduced by the application of the TMD, and that adding an AMD reduces it further. However, for some cases which include an AMD, the displacements of the mass damper are too large to be practical for the control of jacket-type offshore platforms. These displacements can be reduced using a larger mass for the mass damper. However, this solution might not be practical. When only a tendon is used below the deck of the platform, similar reductions in the platform displacements are achieved with a significantly larger control force. When only a propeller thruster is used just below

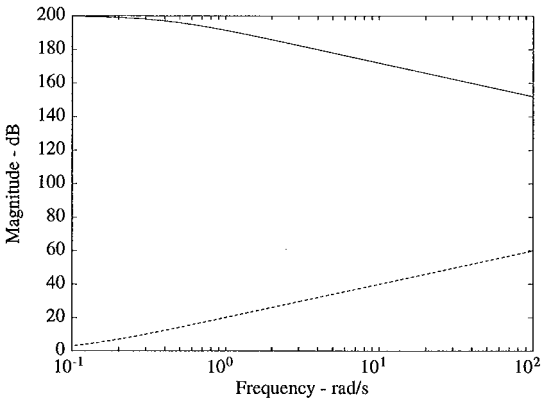

Figure 7. Weighting functions $\alpha_1 W_1$ and $\alpha_2 W_2$ for case III.

the sea water level, the same reductions in the platform displacements are achieved using a significantly smaller control force. The control force produced by the propeller thruster is generally smaller than the control force generated by the tendon control. When a TMD and a tendon below the deck of the platform are used, the control force is smaller than when only a tendon is used, and the displacement of the damper mass is smaller than the displacement of the AMD. Hence it can be seen here that the tendon mechanism helps to reduce the travel distance of the TMD. Therefore, a combination of a TMD and tendon mechanism may allow a smaller mass ratio for the TMD. When a TMD and a propeller thruster just below the sea water level are used, the control force is even smaller than in the previous case. Therefore, this combination is probably the best for controlling the jacket-type offshore platforms considered here.

The dominant periods of ocean waves considered here signify typical waves experienced during the everyday life of the platform and during extreme storm conditions, e.g. the longer the period it represents stormy conditions. It is noted that when the fundamental platform period is separated from the wave dominant period, the waves have considerable background energy around the platform natural periods, thus resulting in large deck displacements. In the case of 18 sec waves, the non-linear drag component also introduces loading at or near third harmonic which falls close or at the natural periods of the platforms under study here. In the cases where the two periods are close, the platform response is dominated by the resonant component. However, in this case the sea state is characterized by lower wave heights, which results in not very large deck displacements. It is in these latter cases that the effectiveness of the control devices is enhanced, which results in more significant reductions in response.

CONCLUSIONS

This paper examines the control of jacket-type offshore platforms using passive/active auxiliary devices. An optimal frequency domain control method based on the minimization of the H_2 norm of the system transfer function is used. The JONSWAP wave spectra has been employed to model the wave surface elevation, from which the wave force spectra was obtained,

including contributions of the nonlinear effects. This wave force spectra was then factorized to give a linear filter for expressing wave load effects in a state-space format which is essential for the control procedure utilized here. A numerical study was conducted in which the displacements of the decks of platforms were controlled by passive and active control mechanisms. The passive control mechanism consisted of a TMD, and the active control devices included an AMD, active tendon mechanism, propeller thrusters, and a combination of these.

The size of the control forces and the reduction in the platform response during different sea states were the primary factors taken into consideration in this study. This study suggests that the combined TMD and propeller thruster mechanism was the most effective means for controlling the jacket-type offshore platforms studied here. For the sea states in which the wave forces were concentrated at frequencies near the dominant frequencies of the platform, the response of the platform was significantly reduced. This study suggests that by including a single or a combination of auxiliary active/passive damping devices, the platform response can be reduced significantly, thus improving both serviceability performance and fatigue life of offshore platforms. The methodology presented here can readily compensate for system time delays and actuator–structure interactions.

ACKNOWLEDGEMENTS

The support for this work was provided in part by the National Science Foundation Grants BCS 90-96274, CMS 95-03779, Office of Naval Research Grant, N 00014-93-1-0761, and several oil companies. The authors are also very grateful to Dr B.F. Spencer, Jr for the discussions regarding structural control. The authors are very thankful to Dr X. Chen for his kind assistance in the preparation of the final manuscript.

APPENDIX A: H_2 CONTROL SOLUTION PROCEDURE

As suggested by the name, H_2 control design is a control design which searches for a stabilizing controller while minimizing the H_2 norm of H_{zd}, $\|H_{zd}\|_2$. The H_2 solution procedure is based on the state-space realization of the system P in Figure 2 in the form

$$\dot{x} = Ax + B_1 d + B_2 u \tag{A1}$$

$$z = C_1 x + D_{12} u \tag{A2}$$

$$y = C_2 x + D_{21} d + D_{22} u \tag{A3}$$

According to Chiang and Safonov [34], the H_2 norm optimal control problem is equivalent to a conventional LQG optimal control problem of the system

$$\dot{x}(t) = Ax(t) + B_2 u(t) + w(t) \tag{A4}$$

$$y(t) = C_2 x(t) + v(t) \tag{A5}$$

with a performance index

$$J = E\left[\int_0^\infty (x(t) \quad u(t)) \begin{pmatrix} Q & X \\ X^{\mathrm{T}} & R \end{pmatrix} \begin{pmatrix} x(t) \\ u(t) \end{pmatrix} \mathrm{d}t\right] \tag{A6}$$

$$= E\left[\int_0^\infty (x^{\mathrm{T}} \quad u^{\mathrm{T}}) \begin{pmatrix} C_1^{\mathrm{T}} \\ D_{12}^{\mathrm{T}} \end{pmatrix} (\, C_1 \;\; D_{12}\,) \begin{pmatrix} x \\ u \end{pmatrix} \mathrm{d}t\right] \tag{A7}$$

and the correlated white plant noise w and white measurement noise v have the joint correlation function

$$E\left[\begin{pmatrix} w(t) \\ v(\tau) \end{pmatrix} (w(t) \quad v(\tau))^{\mathrm{T}}\right] = \begin{pmatrix} S_w & X_f \\ X_f^{\mathrm{T}} & S_v \end{pmatrix} \delta(t-\tau) = \begin{pmatrix} B_1 B_1^{\mathrm{T}} & B_1 D_{21}^{\mathrm{T}} \\ D_{21} B_1^{\mathrm{T}} & I \end{pmatrix} \delta(t-\tau) \tag{A8}$$

The final H_2 optimal controller is the transfer function

$$\dot{x}_{cp} = A_{cp} x_{cp} + B_{cp} y, \quad u = C_{cp} x_{cp} + D_{cp} y \tag{A9}$$

where

$$A_{cp} = A - K_{\mathrm{f}} C_2 - B_2 K_{\mathrm{c}} + K_{\mathrm{f}} D_{22} K_{\mathrm{c}} \tag{A10}$$

$$B_{cp} = K_{\mathrm{f}} \tag{A11}$$

$$C_{cp} = K_{\mathrm{c}} \tag{A12}$$

and

$$D_{cp} = 0 \tag{A13}$$

where K_{c} is the control gain matrix and K_{f} is the Kalman–Bucy filter gain matrix. Both are obtained by solving respective Riccati equations [6].

REFERENCES

1. Kareem A, Kijewski T, Smith CE. Analysis and performance of offshore platforms in hurricanes. *Wind & Structures* 1999; **2**(1): 1–24.
2. Hirayama T, Ma N. Dynamic response of a very large floating structure with active pneumatic control. *Proceedings of the Seventh* (1997) *International Offshore and Polar Engineering Conference*, Honolulu, vol. I, 1997; 269–276.
3. Sirlin S, Paliou C, Longman RW, Shinozuka M, Samaras E. Active control of floating structures. *Journal of Engineering Mechanics*, ASCE 1986; **112**(9): 947–965.
4. Reinhorn AM, Manolis GD, Wen CY. Active control of inelastic structures. *Journal of Engineering Mechanics*, ASCE 1987; **113**(3): 315–333.
5. Yoshida K, Suzuki H, Nam D, Hineno M, Ishida S. Active control of coupled dynamic response of TLP hull and tendon. *Proceedings of the 4th International Offshore and Polar Engineering Conference*, Osaka, Japan, 10–15 April 1994.
6. Suhardjo J, Kareem A. Feasibility of active control of offshore platforms. *Technical Report NDCE* 91-004, Dept. of Civil Engrg & Geological Sciences, University of Notre Dame, Notre Dame, Indiana, 1991.
7. Abdel-Rohman M. Structural control of a steel jacket platform. *Structural Engineering & Mechanics* 1996; **4**(2): 125–138.

8. Nakamura M, Kajiwara H, Koterayama W, Hyakudome T. Control system design and model experiments on thruster assisted mooring system. *Proceedings of the Seventh* (1997) *International Offshore and Polar Engineering Conference*, Honolulu, May 25–30, 1997; 641–648.
9. Yamamoto I, Matsuura M, Yamaguchi Y, Shimazaki K, Tanabe A. Dynamic positioning system based on nonlinear programming for offshore platforms. *Proceedings of the Seventh* (1997) *International Offshore and Polar Engineering Conference*, Honolulu, May 25–30, 1997; 632–640.
10. Soong TT. State-of-the-art review: active control in civil engineering. *Engineering Structures* 1988; **10**: 74–84.
11. Housner G, Bergman LA, Caughey TK, Chassiakos AG, Claus RO, Masri SF, Skeleton RE, Soong TT, Spencer BF, Yao JTP. Structural control: past, present, and future. ASCE, *Journal of Engineering Mechanics* 1997; **123**(9): 897–971.
12. Kijewski T, Kareem A, Tamura Y. Overview of methods to mitigate the response of wind-sensitive structures. *Proceedings of Structural Engineering World Congress*, July 19–23, San Francisco, Elsevier: Amsterdam, 1998 (Hard copy abstract volume and full-length paper on CD-ROM).
13. Kareem A, Kijewski T, Tamura Y. Mitigation of motions of tall buildings with specific examples of recent applications. *Wind & Structures* 1999; **2**(3): 201–251.
14. Petersen NR. Design of large scale tuned mass dampers. In *Structural Control*, Liepholz HH (ed.). North-Holland: Amsterdam, 1980; 581–598.
15. Suhardjo J. Frequency domain techniques for control of civil engineering structures with some robustness considerations. *Ph.D. Dissertation*, University of Notre Dame, Notre Dame, Indiana, 1990.
16. Suhardjo J, Spencer BF, Kareem A. Frequency domain optimal control of wind excited buildings. *Journal of Engineering Mechanics*, ASCE 1992; **118**(12): 2463–2481.
17. Spencer Jr BF, Suhardjo J, Sain MK. Frequency domain optimal control strategies for aseismic protection. *Journal of Engineering Mechanics* 1994; **120**(1): 135–158.
18. Suhardjo J, Kareem A. Structural control of offshore platforms. *Proceedings of the Seventh International Offshore and Polar Engineering Conference*, ISOPE-97, Honolulu, May 25–30, 1997.
19. Suhardjo J, Spencer BF, Sain MK. Feedback–feedforward control of structures under seismic excitation. *Structural Safety* 1990; **8**: 69–89.
20. Yamada K, Kobori T. Linear quadratic regulator for structure under on-line predicted future seismic excitation. *Earthquake Engineering and Structural Dynamics*, 1996; **25**: 631–644.
21. Mei G, Kareem A, Kantor JC. Real-time model predictive control of structures under earthquakes. *Proceedings of the Second World Conference on Structural Control*, Kyoto, Japan, June 28–July 2, vol. 2, 1998.
22. Chakrabarti SK. *Hydrodynamics of Offshore Structures*. Springer: New York, 1987.
23. Roberts JB, Spanos PD. *Random Vibration and Statistical Linearization.* Wiley: New York, 1990.
24. Soong TT, Grigoriu M. *Random Vibration of Mechanical and Structural Systems*. Prentice-Hall, Inc: New Jersey, 1993.
25. Borgman LE. Random hydrodynamic forces on objects. *Annals of Mathematical Statistics* 1967; **38**: 37–51.
26. Li Y, Kareem A. Stochastic response of a tension leg platform to wind and wave fields. *Journal of Wind Engineering and Industrial Aerodynamics* 1990; **36**: 915–920.
27. Kareem A, Hsieh CC, Tognarelli MA. Frequency domain analysis of offshore platforms in non-Gaussian seas. *Journal of Engineering Mechanics*, ASCE 1998; **124**(6): 668–683.
28. Spanos P-TD. Filter approaches to wave kinematics approximation. *Applied Ocean Research* 1986; **8**(1): 2–7.
29. Li Y, Kareem A. Parametric modeling of stochastic wave effects of offshore platforms. *Applied Ocean Research* 1993; **15**: 63–83.
30. Li Y, Kareem A. Multivariate Hermite expansion of hydrodynamic drag loads on tension leg platforms. *Journal of Engineering Mechanics*, ASCE 1993; **119**(1): 91–112.
31. Tognarelli MA, Zhao J, Rao KB, Kareem A. Equivalent statistical quadratization and cubicization for nonlinear systems. *Journal of Engineering Mechanics*, ASCE 1997; **122**(5): 512–523.
32. Davis MC. Factoring the spectral matrix. *IEEE Transactions on Automatic Control* 1963; **8**(4): 296–305.
33. Kareem A. Mitigation of wind induced motion of tall buildings. *Journal of Wind Engineering and Industrial Aerodynamics* 1983; **11**: 273–284.
34. Chiang RY, Safonov MG. *Robust-Control Toolbox.* The Math Works: South Natick, Massachusetts, 1988.

